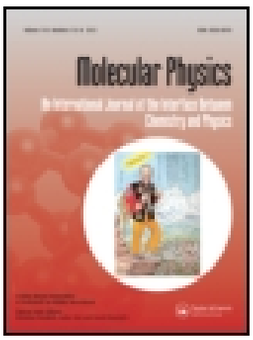

Taylor & Francis
Taylor & Francis Group

Molecular Physics

An International Journal at the Interface Between Chemistry and Physics

ISSN: 0026-8976 (Print) 1362-3028 (Online) Journal homepage: https://www.tandfonline.com/loi/tmph20

Vibrationally exciting molecules trapped on a microchip

Mark J. Abel , Silvio Marx , Gerard Meijer & Gabriele Santambrogio

To cite this article: Mark J. Abel , Silvio Marx , Gerard Meijer & Gabriele Santambrogio (2012) Vibrationally exciting molecules trapped on a microchip, Molecular Physics, 110:15-16, 1829-1837, DOI: 10.1080/00268976.2012.683885

To link to this article: https://doi.org/10.1080/00268976.2012.683885

Published online: 11 May 2012.

Molecular Physics
Vol. 110, Nos. 15–16, 10–20 August 2012, 1829–1837

Taylor & Francis
Taylor & Francis Group

INVITED ARTICLE

Vibrationally exciting molecules trapped on a microchip

Mark J. Abel, Silvio Marx, Gerard Meijer and Gabriele Santambrogio*

Fritz-Haber-Institut der Max-Planck-Gesellschaft, Faradayweg 4-6, 14195 Berlin, Germany

(*Received 10 January 2012; final version received 28 March 2012*)

Polar molecules in selected quantum states can be guided, decelerated and trapped using electric fields created by microstructured electrodes on a chip. Here we demonstrate that transitions between two vibrational quantum states can be induced while the molecules are trapped above the chip. We use CO molecules, prepared in the $J=1$ rotational level of the $a^3\Pi_1$, $v=0$ state and induce the transition to either the $J=1$ or the $J=2$ level in the vibrationally excited $a^3\Pi_1$, $v=1$ state with pulsed, narrowband IR radiation. First, the vibrational excitation is studied using CO molecules in a freely propagating molecular beam, in a well-defined homogeneous electric field. Then, we demonstrate that the IR radiation can be coupled to CO molecules that are trapped less than 50 μm above the chip by guiding molecules in the $v=0$ level to the center of the chip where they are pumped to the $v=1$ level. The molecules remain trapped and are then guided off the chip and state-selectively detected.

Keywords: Stark decelerator; polar molecules; microchip; carbon monoxide; vibrational excitation

1. Introduction

The manipulation of polar molecules above a chip using electric fields produced by microstructured electrodes on the chip surface is an emerging research field [1–4]. Many of the advantages of magnetic atom chips [5,6] could also be realized with electric molecule chips: miniaturization of field structures enables the creation of large field gradients, i.e., large forces and tight potential wells for polar molecules. Above a chip, the positions of these potential wells, and thereby the positions of the trapped molecules, can be controlled to an extreme precision. At the same time, though, one has to realize that molecule chips are still in their infancy and that their potential still needs to be explored.

Molecules on a chip can be coupled to photons over a wider range of frequencies than atoms. The fundamental molecular vibrational modes can be addressed with mid-infrared photons whereas their overtones and combination modes extend into the near-infrared range. In addition, polar molecules have a dense set of rotational transitions in the sub-THz, or mm-wave, region of the spectrum. Being able to induce a transition to another internal quantum state in the molecule is particularly interesting when the molecule remains trapped in the final state as well. Recently, we have demonstrated that transitions between adjacent rotational levels within a given electronic and vibrational state can be induced above the chip; these transitions were driven with high efficiency using a coherent, narrowband continuous-wave source of radiation with a wavelength of around 1.5 mm [7].

In this paper we describe our experiments demonstrating that vibrational transitions can be induced in molecules on a chip. The system we use is the carbon monoxide molecule, prepared with a pulsed laser in a single rotational level ($J=1$) of its first electronically excited, metastable state ($a^3\Pi_1$, $v=0$). The $v=1 \leftarrow v=0$ vibrational transition is induced using pulsed IR radiation around 5.9 μm. Molecules prepared in selected rotational levels of the vibrationally excited $v=1$ state are subsequently state-selectively detected using ionization with another pulsed laser system.

The paper consists of two parts. In the first part, the experimental setup is described and the vibrational excitation step is characterized using experiments on a freely propagating molecular beam of CO molecules in a homogeneous electric field. This sets the stage for the discussion of the IR excitation of CO molecules in the miniaturized electric field traps, where the molecules are exposed to an inhomogeneous, rotating electric field. In the second part, experiments are described in which the pulsed IR radiation interacts with the metastable CO molecules while these are propagating with a constant velocity at a close distance above the chip. These experiments demonstrate that the pulsed IR radiation can be coupled onto the chip without damaging the chip and that the CO molecules – guided

*Corresponding author. Email: Gabriele.Santambrogio@fhi-berlin.mpg.de

ISSN 0026–8976 print/ISSN 1362–3028 online

http://dx.doi.org/10.1080/00268976.2012.683885
http://www.tandfonline.com

in moving electric field traps to the center of the chip while in the $v=0$ state – can be pumped to the $v=1$ state while on the chip. The vibrationally excited molecules remain confined in the miniaturized electric field traps, are transported to the end of the chip and detected.

2. Setup of the experiment

The experimental setup is shown schematically in Figure 1. We begin the experiments by allowing a mixture of 20% $^{12}C^{16}O$ in Kr, cooled to 140 K, to expand into vacuum through a pulsed solenoid valve. The expansion is skimmed to form a collimated beam with a mean velocity of 330 m/s and intersected at right angles by a 206 nm laser pulse exciting the molecules from the ground electronic state to the lowest vibrational level of the lowest metastable triplet electronic state, $a^3\Pi$, as shown in Figure 2. We select the middle spin–orbit level with $|\Omega|=1$, because these transitions are more than 40 times more intense than transitions to the other spin–orbit components [8]. The laser provides about 0.5 mJ in a 5 ns pulse with a measured bandwidth of about 200 MHz. Even in the presence of parity-mixing stray fields, this narrow bandwidth allows for the selective excitation of the upper component of the $v=0$, $J=1$ Λ-doublet. This half of the Λ-doublet consists of two degenerate low-field seeking sublevels (that is, their Stark energy increases with increasing electric field) having projection quantum numbers $M=\pm1$ and a single sublevel ($M=0$) with no first-order Stark shift. If the molecules are excited before the skimmer, collisions populate the lower Λ-doublet levels to some extent; if the excitation occurs in the fully-formed supersonic beam, the absence of collisions hinders population redistribution. The $a^3\Pi_1$, $v=0$, $J=1$ state has a lifetime of 2.6 ms [8], long enough for all experiments presented here.

The excited molecules fly freely over a distance of 127 mm to the chip, which consists of an array of 1848 equidistant gold electrodes deposited on a 1 mm thick flat glass substrate. We define the y-axis of a right-handed coordinate system as the direction normal to the chip surface. The z-axis is the direction of propagation of the molecular beam. Each of the 1848 electrodes is 4 mm long in the x-direction, 10 μm wide in the z-direction and approximately 100 nm thick. They are deposited onto the substrate with a 40 μm center-to-center spacing, forming a structure that is 74 mm long (*Micro Resist Technology GmbH*). The electrodes are arranged in groups of six and when the appropriate voltages are applied, two minima of electric field strength are formed over each group – i.e., the minima are spaced by 120 μm along the z-direction. For the voltages used in the experiments, these minima occur at a distance above the chip $y_{\min}=24.5$ μm, with a saddle point in the y–z plane occurring at $y_{\rm sp}=46.3$ μm. These periodic minima in electric field strength act as tubular traps for molecules in low-field seeking states. Because we are only

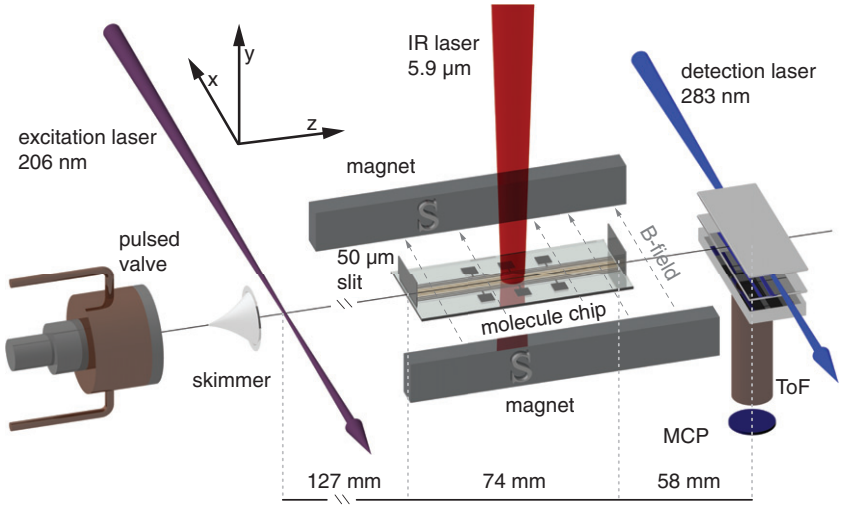

Figure 1. Molecular beam machine. After a skimmer, a beam of CO molecules is prepared in selected rotational levels of the $a^3\Pi_1$ $v=0$ state using 206 nm radiation. They fly 127 mm to the chip entrance. If they pass through a 50 μm slit and over the molecule chip, they can be trapped in electric field minima. In the center of the 74 mm long chip, they can be vibrationally excited by an infrared laser with a wavelength near 5.9 μm. After being ejected from the chip, the molecules fly 58 mm to a time-of-flight detector where they are state-selectively ionized and detected. A 190 gauss magnetic field around the chip prevents non-adiabatic losses from the traps.

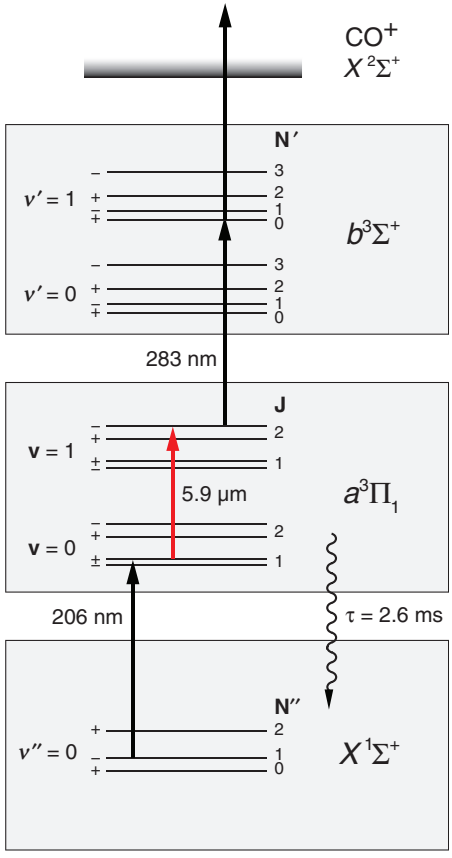

Figure 2. Partial level scheme of CO. Molecules are pumped with 206 nm radiation from the ground electronic state ($X^1\Sigma^+$) to $v=0$ in the lowest-lying triplet state, $a^3\Pi_1$. Either the $J=1$ or the $J=2$ Λ-doublet can be selectively accessed in this way. Molecules in the $v=0$, $J=1$ levels are excited by mid-IR light near 5.9 μm to the $v=1$ level. The $v=0$ or 1 vibrational levels in the $a^3\Pi_1$ state can be state-selectively ionized in a two-photon process via the $v'=0$ or 1 levels respectively in the $b^3\Sigma^+$ state.

interested in detecting molecules that interact with the traps, we place a slit at the entrance to the chip which allows only those molecules with $y<50$ μm to pass [2].

By sinusoidally modulating the voltages applied to the chip electrodes, the traps can be made to travel smoothly along the chip in the z-direction at a constant height and without changing their shape [1]. The speed of the traveling traps is determined by the electrode spacing and the frequency of the modulation. A waveform of 2.75 MHz frequency will move the traps at 330 m/s, the mean velocity of the free molecular beam. An amplitude of 180 V creates 65 mK deep traps for CO molecules in low-field seeking components of the $a^3\Pi_1$, $v=0$, $J=1$ level, corresponding to the kinetic energy of a CO molecule traveling at about 6 m/s. Under these conditions, any molecule in the appropriate quantum state traveling at 330±6 m/s has the chance to be stably guided across the chip inside a trap, but those molecules traveling at higher or lower speeds experience – in their moving frame of reference – a rapidly varying corrugated potential which on average repels them from the surface of the chip. These rejected molecules are blocked from reaching the detector when they fail to pass a second 50 μm slit. A 190 gauss offset magnetic field, pointing across the chip surface in the x-direction, provides a small Zeeman splitting at zero electric field that significantly improves guiding efficiency by suppressing non-adiabatic transitions to non-trappable states [9].

Importantly for the modeling of the experimental results, the electric field vectors which form the trap have a distorted quadrupole geometry. As the voltages are modulated and the traps move, the electric field vectors and thus the axes of the quadrupole rotate relative to the (moving) center of the trap in the y–z plane at 3/2 the frequency of the sinusoidal waveforms. The trapping potential is a result of the Stark energy of the molecules, which depends on electric field strength only and not on electric field direction. However, the time- and space-varying direction of the electric field makes the excitation efficiency for the trapped molecules time- and position-dependent. This will be considered in more detail in Section 3.

When the molecules are in the center of the microchip, they are addressed with tunable IR radiation (~200 μJ pulses with ~4 ns duration and 2.5 GHz bandwidth, *Sirah Laser- und Plasmatechnik GmbH*). This radiation is created by first generating the difference frequency between the output of a nanosecond dye laser (bandwidth ~1.5 GHz) and part of the fundamental of an injection-seeded Nd : YAG laser. This narrowband difference frequency light, with wavelength near 3 μm, is parametrically amplified by a second portion of the Nd : YAG fundamental. Finally, the signal and idler waves are mixed in a AgGaSe crystal to generate their difference frequency [10]. Long-duration frequency stability of the mid-infrared output requires that the seeder frequency of the Nd : YAG laser be stabilized, for which we use a molecular iodine reference and a feedback loop with an approximately 1 second response time. Also, the 2.5 GHz linewidth we measure is an average of typically a few thousands of laser shots. The width therefore reflects not only the inevitable spectral broadening and temporal narrowing accompanying nonlinear conversion, but also the statistical variation of the dye laser output wavelength from shot to shot. This wavelength fluctuates randomly, switching between about three longitudinal modes of the dye laser resonator. To achieve a significantly narrower linewidth it would be necessary to either insert a

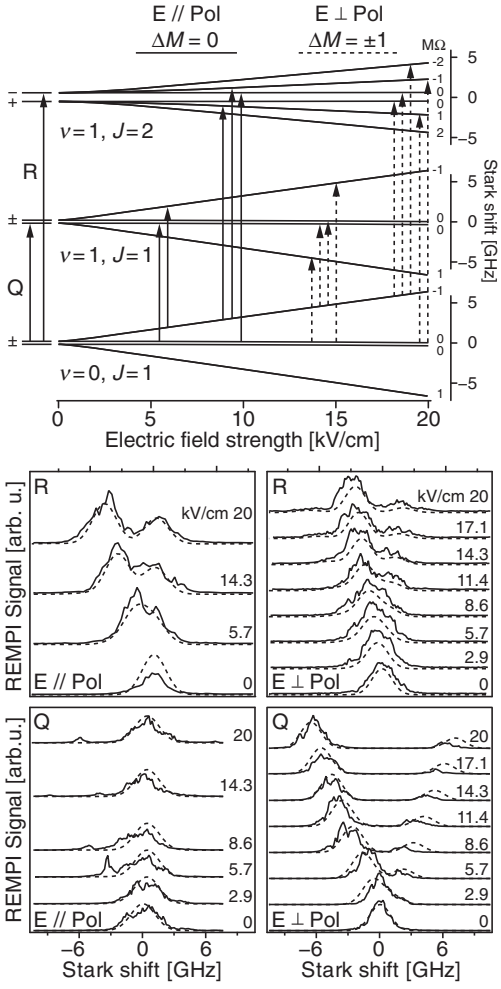

Figure 3. Stark shifted rotational states in the $v=0$ and $v=1$ manifolds of the $a^3\Pi_1$ state. The top panel shows the calculated Stark curves for all the components of $v=0$, $J=1$ and $v=1$, $J=1$ and 2. The arrows indicate allowed transitions in the Q- and R-branches when the laser polarization is either parallel (solid) or perpendicular (dashed) to a strong applied electric field. On the left-hand side are the field-free energy levels and transitions, while on the right-hand side the quantum numbers of the mixed eigenstates are given. The bottom panels show four series of Stark spectra for increasing electric field – the same four cases as indicated with arrows in the top panel. In these spectra, the solid curves are the measured data and the dashed curves are the simulation.

scannable etalon into the laser oscillator, or to seed the dye amplifier with CW light. We have not attempted either approach; in fact, as will be seen below, the bandwidth of 2.5 GHz is close to an optimal value for the experiments we describe here. The spot of the IR beam on the chip is more or less round, with 2 mm size (FWHM).

Two ro-vibrational transitions are allowed from the $a^3\Pi_1$ $v=0$, $J=1$ state to the $a^3\Pi_1$ $v=1$ state: excitation either to the $J=1$ level (Q-branch) or to the $J=2$ level (R-branch) with frequencies given in References [11,12]. The latter transition is sketched in Figure 2. The linewidth of the IR laser is much larger than either of the two Λ-doublet splittings. In an electric field, these transitions are split into multiple Stark-shifted components. The molecules are then guided off the chip and state-selectively detected by resonance-enhanced multiphoton ionization (REMPI) via the $b^3\Sigma^+$ state. We use ionization through $b^3\Sigma^+$, $v=1$, $N'=2 \leftarrow a^3\Pi_1$, $v=1$, $J=1$ or 2 to probe the population after Q- or R-branch excitation, respectively. One possible REMPI transition, originating in the $v=1$, $J=2$ level of the $a^3\Pi_1$ state, is also shown in Figure 2. The linewidth of the ionizing laser is less than one wavenumber, sufficient to resolve individual rotational transitions.

3. Spectroscopy of CO in the $a^3\Pi_1$ state

Replacing the chip with a pair of metal plates to provide a homogeneous electric field allows us to measure the field-dependent vibrational absorption spectrum of the metastable CO molecules. The resulting absorption spectra are shown in Figure 3 for the cases of the IR light polarized parallel and perpendicular to the applied field, and for field strengths between 0 and 20 kV/cm.

Most of the Stark splitting comes from mixing between the closely spaced, opposite-parity components of the same Λ-doublet. To a good approximation, then, the electric-field-dependent energies of these Λ-doublet levels can be written as:

$$U(|\vec{E}|) \simeq \pm\sqrt{\left(\frac{E_\Lambda}{2}\right)^2+\left(\mu|\vec{E}|\frac{M\Omega}{J(J+1)}\right)^2}. \qquad (1)$$

In this equation, E_Λ is the magnitude of the Λ-doublet splitting (394 MHz for $J=1$ and 1151 MHz for $J=2$ [13]) and $\mu M\Omega/J(J+1)$ is the magnitude of the projection of the body-fixed dipole moment $\mu=1.375$ Debye [13,14] on the electric field, $\vec{E}$.

The Stark curves calculated using Equation (1) for electric field strengths from 0 to 20 kV/cm are shown in Figure 3. As already mentioned, after excitation by the 206 nm laser only the upper Λ-doublet components of $v=0$, $J=1$ are populated. At zero electric field, the parity is well-defined and as a result molecules excited in a Q-branch transition always end in the lower Λ-doublet component of the $v=1$, $J=1$ state. By contrast, the parity selection rule in R-branch transitions ensures that at zero field, only transitions to the upper components of the $v=1$, $J=2$ Λ-doublet are

allowed. As the external electric field increases, the parity of the eigenstates progressively mixes and the eigenstates begin to have a well-defined product of quantum numbers $M\Omega$. When the dipole term dominates the Λ-doubling term in Equation (1), the parity of the eigenstates is totally mixed and both Λ-doublet components can be reached during vibrational excitation. In such a strong field, the product $M\Omega$ is well-defined for each eigenstate. Note that parity is always well-defined for the $M=0$ levels because to first order they experience no Stark shift.

The vertical arrows in the top panel of Figure 3 show the allowed transitions when the infrared laser polarization is turned parallel or perpendicular to the applied electric field, and corresponding to the experimental situation in which only the upper component of the Λ-doublet of the $v=0$, $J=1$ level is populated. When the laser polarization and applied electric field are parallel, transitions with $\Delta M=0$ are allowed, whereas when the polarization and field are perpendicular the laser drives $\Delta M=\pm 1$ transitions. Also shown in Figure 3 are the allowed transitions in the field-free case.

Small corrections to this simple picture arise because of second-order interactions, so a Hamiltonian including the spin–orbit splitting, nuclear rotation, Λ-doubling, spin–spin interaction, and the explicit form of the Stark interaction is used to quantitatively model the measured spectra. Detailed information on these interactions and the calculation of their matrix elements can be found in References [15,16]. To simulate the Stark spectra, this Hamiltonian is diagonalized for each electric field strength, then the positions, intensities, and final states for all possible transitions originating in the upper component of the Λ-doublet with $v=0$, $J=1$ are calculated using the transition dipole operators $\hat{\mu}_z$ or $\hat{\mu}_x$ (the IR beam propagates in the negative y-direction so $\hat{\mu}_y \cdot \vec{E}_{IR}=0$). The resulting 'stick spectra' are convoluted with a Gaussian function of 2.5 GHz width, corresponding to the experimentally measured linewidth of the IR laser. The calculated frequencies and intensities of the resonances are in good agreement with the measurements, whose major limitation is the uncertainty in the laser polarization direction with respect to the electric field. This will lead to contributions in the spectra from nominally forbidden transitions; these contributions are particularly evident in the Q-branch spectra for the case when the polarization is nominally parallel to $\vec{E}$. Because the maximum electric field strength experienced by trapped molecules on the chip is about 4.7 kV/cm, the bandwidth of the IR laser is wide enough to address all possible upper states in either $v=1$, $J=1$ or $v=1$, $J=2$ levels, albeit possibly with different intensity than that observed in the situation of a homogeneous field.

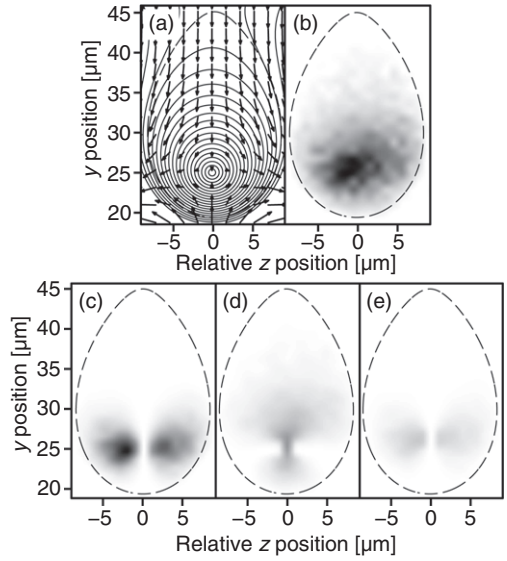

Figure 4. Spatial distributions of molecules in the traps. One configuration of electric field in the trap is shown in (a), along with the contours of equal electric field strength (solid curves). The dashed contour line is the limit of the trap; outside of this spatial region the molecules cannot be trapped. Trajectory simulations yield the relative density (b) of $v=0$, $J=1$ molecules in the traps 495 μs after the 206 nm laser fires; this corresponds to molecules in the center of the chip. The boundary of the trap is again shown by the dashed curve. The relative densities of molecules excited to (c) $v=1$, $J=1$; (d) $v=1$, $J=2$, $M\Omega=-2$; and (e) $v=1$, $J=2$, $M\Omega=-1$ are shown together with the boundary of the trap. While panels (c), (d), and (e) are plotted with the same linear intensity scale, they are not directly comparable to the scale of panel (b) because the overall excitation efficiency of the IR laser is not accurately known.

The electric field in the region of a trap above the chip is shown in Figure 4(a), which also shows the equal-field-strength contours of the trap. The saddle point of electric field strength at $z=0$, $y=46.3$ μm determines the depth of the trap, since a molecule with kinetic plus potential energy exceeding the Stark energy at the saddle point will (given enough time) find its way out. Also shown is the egg-shaped rim of the trap, the contour where the electric field strength is equal to the strength at the saddle point. To find the density distribution of molecules in the trap in the center of the chip where the infrared excitation takes place, we performed classical trajectory simulations [2]. The density distribution of metastable CO molecules guided to the center of the chip in the $v=0$, $J=1$, $M\Omega=-1$ levels is shown in Figure 4(b). We note that the simulated distribution is not evenly spread through the trapped portion of phase space – particularly, the spread of y-positions is smaller than that of a totally

filled trap. This results from the under-filling of the v_y-dimension of phase space at the entrance of the chip inherent to the current setup of the molecular beam machine [4]. Further, the trapped phase space distribution is incompletely randomized by the time the molecules arrive at the center of the chip.

Now we consider infrared transitions of trapped $v=0$, $J=1$, $M\Omega=-1$ molecules in the presence of a variable quantization axis against which the fixed polarization of the IR laser must be compared. For an incoming IR beam traveling in the negative y-direction, there are two polarization directions of the IR laser that we could use: along the x- and z-directions. No matter how they rotate, the electric field vectors of the trap always lie in the y–z plane, making them always perpendicular to the electric field of x-polarized light. In this case, Q-branch excitation does not lead to trapped final states. If the light is z-polarized, however, the two fields will be parallel in some regions of the trap and perpendicular in others. For this case, excitations in both the Q-branch and the R-branch can end in trappable states, and it is this case that we consider in detail next.

As for the case of the Stark spectroscopy experiments on the free beam we calculate the energy levels and eigenstates of the molecule in the electric field on the chip by diagonalizing the molecular Hamiltonian, but now generating different eigenfunctions and transition probabilities at each point in space. Combining the simulated density with the spectroscopic calculations, we can predict the spatial variation of the excitation efficiency into each rotational level and sublevel in the $v=1$ manifold. Figure 4(c) shows the distribution of CO molecules excited to the $v=1$, $J=1$, $M\Omega=-1$ state immediately after the IR laser pulse. Because the trap shape does not change during this IR excitation, all of these molecules will be stably guided to the end of the chip and will therefore be detected. However, the Stark interaction decreases by 1/3 on excitation to the $J=2$, $M\Omega=-2$ levels (and by 2/3 for the $J=2$, $M\Omega=-1$ levels, see Equation (1)) and so some formerly trapped molecules are lost after IR excitations in the R-branch. Figures 4(d) and (e) show the subset of molecules just after the IR laser pulse arrives which are both excited to the $v=2$, $J=2$, $M\Omega=-2$ and $M\Omega=-1$ levels, respectively, and which will arrive at the detector.

The shapes of the distributions come about because the transition strength depends on the projection of the laser polarization on the trap field and is therefore proportional to either $\cos^2(\theta)$ ($\Delta M=0$) or $\sin^2(\theta)$ ($\Delta M=\pm 1$), where θ is the angle between the trap field and the laser polarization. When the trap fields rotate the total excitation probability into each excited state can change by up to $\pm 20\%$ because neither the trap nor the molecule distribution are symmetric under rotations in the y–z plane. In the guiding experiments described below, we make sure that the IR laser timing is scanned in steps incommensurate with the waveform period to average over trap field rotations.

We know from guiding experiments in the $v=0$ state that in the present experimental configuration about 5% of the signal is due to metastable CO molecules in the $M=0$ states [7]. Although some of these molecules are probably excited to the trappable $M\Omega=-1$ state by the IR laser, at the instant the laser fires few of them will find themselves at the right position to be trapped and subsequently guided off the chip. We neglect this small fraction of molecules in our calculations.

4. Guiding experiments

When the chip field is turned off, the free-flying molecules have a wide velocity distribution. The molecules' arrival time distribution at the REMPI detector, measured by scanning the Q-switch trigger time of the ionizing laser, is shown in Figure 5(a). This distribution, centered at 790 μs with 55 μs FWHM, corresponds to a velocity distribution centered at 330 m/s with 20 m/s FWHM. Because of the velocity distribution, the initial 2 mm packet (given by the 206 nm laser spot size) spreads considerably during its flight through the machine. In the middle of the chip the packet is 8 mm long, and by the time it reaches the REMPI detector it is roughly 14 mm long (FWHM) – if flying freely. Since the IR and REMPI laser spots are about 2 mm and 1.2 mm, respectively, these two lasers together act as a velocity filter. Only when they are timed to address the same portion of the expanding packet can one detect vibrationally excited molecules. To address the entire packet of free-flying molecules with both lasers we scan the IR and the REMPI lasers with two different timesteps. The timestep used to scan each laser is proportional to the size of the packet of molecules at the position of that laser beam. This measurement, shown in red in Figure 5(a), is virtually identical to that of the free-flying molecules in the $v=0$ state. When the chip waveforms are turned on at 2.75 MHz, molecules with velocities different from 330 m/s are selectively repelled from the chip surface, resulting in a dramatically narrowed arrival time distribution. For example, molecules guided in the $v=0$, $J=1$ level, that is, with no IR radiation present, are shown overlaid on the free-flying signals in Figure 5(a). We note that because the molecule chip manipulates the forward velocity of the CO molecules as they traverse

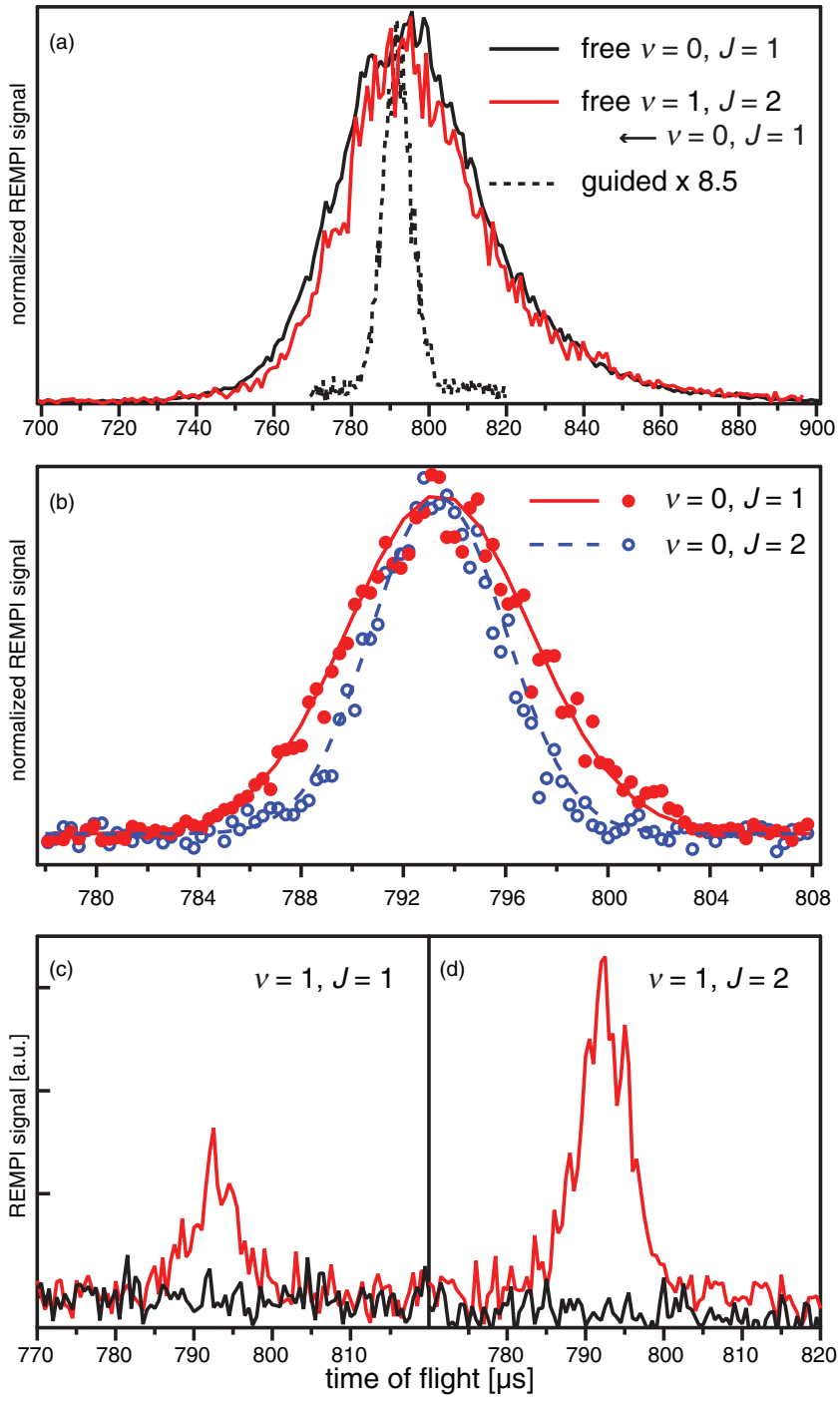

Figure 5. Arrival time distributions of CO molecules, guided and unguided. Shown in solid lines in panel (a) are free flying $v = 0$ molecules (black) and free-flying molecules which are transferred to $v = 1$ at the center of the chip (red). The dashed line in panel (a) shows molecules in the $v = 0$, $J = 1$ state guided across the chip. (b) Experimental measurement (markers) and trajectory simulations (lines) of $v = 0$, $J = 1$ (red disks) and $v = 0$, $J = 2$ (blue circles) molecules guided at 330 m/s. The arrival time distributions of guided molecules in the $v = 1$, $J = 1$ and $J = 2$ states pumped from the $v = 0$, $J = 1$ state with (red) and without (black) the IR laser are shown in panels (c) and (d), respectively.

the experiment, there is no straightforward conversion between arrival time and molecular velocity, except in the case of the free beam.

The phase space acceptance of the chip decelerator for molecules in trappable states is strictly related to the trap depth: for deeper traps a larger portion of the incoming velocity distribution will be accepted in each trap and a larger number of traps will be filled. This, in turn, manifests in a wider time of flight distribution at the REMPI detector because the packet of molecules leaving the chip is both longer (more microtraps are filled) and spreads more during its flight to the detector. We use this fact as an experimental probe of the trap depth by validating the trajectory simulation results (convoluted with the 1.2 mm FWHM ionization laser spot size) against the measured data. Figure 5(b) shows the measured and simulated arrival time distribution of molecules guided at 330 m/s when the 206 nm laser is used for preparation in the $v=0$, $J=1$ or 2 levels.

The background level is related to molecules in the $M=0$ levels. Since they do not interact with the chip fields, these molecules fly unhindered across the chip even when the waveforms are on and arrive at the detector with the same arrival time distribution as unguided molecules. In the guided peaks of Figures 5(a) and (b), one can see that molecules in the $M=0$ levels contribute very little to the observed signal: the unguided background is at its highest only a few percent of the guided peak.

When the IR laser is used to promote the trapped molecules to either $J=1$ or $J=2$ in the $v=1$ level from $J=1$, $v=0$, the arrival time distributions shown in Figures 5(c) and (d) result. The red lines show the relative number of vibrationally excited molecules arriving at the detector when the IR laser is present; the black curves show what happens when the IR laser is blocked, indicating that there is no contamination of the vibrationally excited signal by metastable molecules in the $v=0$ level. These data clearly show that trapped $v=0$ molecules may be excited by infrared radiation while flying close to the surface of the microchip. In particular, the widths of the arrival time distributions can be compared to the free-flying $v=1$ molecules in Figure 5(a). We roughly estimate the efficiency of infrared excitation to be about 10%.

Trajectory simulations indicate that molecules promoted to the $M=0$ levels have only one tenth the probability of reaching the detector than those promoted to low-field seeking levels do. For the case of a Q-branch transition, the relative probability of excitation in the trap to $M=0$ states is about 50%. Therefore we conclude that the signal consists of less than 10% $M=0$ molecules. This number is reduced to about 0.5% for R-branch transfer. Additionally, molecules that are promoted to low-field seeking states but not trapped are repelled from the chip surface. They are blocked by the 50 μm slit and do not contribute to the measured signal. Molecules promoted to high-field seeking states are attracted to the chip, crashing into the surface.

So far, we have been considering one-photon transitions of molecules trapped on the chip. Now we briefly consider an alternative approach to populate low-field seeking states. As discussed in Section 3, in a strong electric field the selection rules for excitation of various M-states depend on the angle between the polarization of the laser and the electric field. In the middle of the trap, however, the field is weak (or nonexistent) and the parity of the upper and lower portions of the Λ-doublet are not totally mixed (or not mixed at all). In this spatial region two electric dipole transitions are needed to connect the low-field seeking positive-parity levels of $v=0$, $J=1$ and $v=1$, $J=1$. One possible way to do this is to use an optical transition to an electronic state that fluoresces quickly on the timescale of trap motion. A good candidate is the $b^3\Sigma^+$ state, which has a lifetime of about 86 ns and decays primarily by fluorescence back to the $a^3\Pi_1$ state [17]. If the transition to the $b^3\Sigma^+$ state is saturated, and assuming a Franck–Condon factor of 0.33 [18] to the $a^3\Pi_1$ $v=1$ level, about 16% of the excited molecules will be distributed over various rotational states in the $v=1$ manifold. Exciting to the $N'=1$ level in the $b^3\Sigma^+$ state, which has negative parity, means that only $J=1$ and $J=3$ are populated on fluorescence in the field-free region at the center of the trap, while $J=2$ is also populated in the parts of the trap where a field is present. An overall transition efficiency of a few percent could be hoped for. We have briefly tested this scheme but obtained about an order of magnitude fewer molecules in the vibrationally excited $J=1$ level than with direct IR pumping.

Finally, it is worth considering the effect of the 190 gauss magnetic field across the chip. While the Zeeman shift from this field is small compared to the Stark shift in the edges of the trap, in the middle of the trap it is larger than the (vanishing) Stark shift. The Zeeman shift is 0.466 MHz/gauss for ^{12}CO $a^3\Pi_1$, $v=1$, $J=1$[9], amounting to a splitting of 89 MHz in our setup. We estimate that the Zeeman interaction is more important than the Stark interaction only within a 1.1 μm radius about the trap center, containing only 4.5% of the total trapped molecules. Therefore, aside from

preventing non-adiabatic transitions, the magnetic field is not expected to have a measurable effect on the experiments described here.

5. Conclusion

In these experiments, we have studied vibrational excitation of molecules trapped on a microchip. CO molecules prepared in selected quantum states were loaded onto the chip directly from a supersonic beam and guided in micrometer-sized electric field traps. While in the traps, they were vibrationally excited by a narrowband infrared laser and subsequently guided off the chip for state-selective detection via REMPI. For understanding quantum transitions of molecules trapped by inhomogeneous fields, the interplay between the pumping field and the trapping field needs to be taken into account. For this purpose, we also studied the spectroscopy of free-flying CO molecules in the $a^3\Pi_1$ state in a homogeneous electric field. We then extended our model of the Stark spectra in a homogeneous field to the more complicated case of the inhomogeneous, rotating field of our microtraps. Depending on the polarization direction of the laser, different transitions can be addressed. We demonstrated population transfer between trapped states in different vibrational levels using two of these transitions.

Acknowledgements

This work has been funded by the European Community's Seventh Framework Program FP7/2007-2013 under grant agreement 216774, and ERC-2009-AdG under grant agreement 247142-MolChip. We acknowledge fruitful discussions with Samuel A. Meek. M.J.A. gratefully acknowledges the support of the Alexander von Humboldt Foundation.

References

[1] S. Meek, H. Bethlem, H. Conrad and G. Meijer, Phys. Rev. Lett. **100**, 1 (2008).
[2] S.A. Meek, H. Conrad and G. Meijer, New J. Phys. **11**, 055024 (2009).
[3] S.A. Meek, H. Conrad and G. Meijer, Science **324**, 1699 (2009).
[4] A.I. González-Flórez, S.A. Meek, H. Haak, H. Conrad, G. Santambrogio and G. Meijer, Phys. Chem. Chem. Phys. **13**, 18830 (2011).
[5] J. Reichel, Appl. Phys. B: Lasers and Optics **74**, 469 (2002).
[6] J. Fortàgh and C. Zimmermann, Rev. Mod. Phys. **79**, 235 (2007).
[7] G. Santambrogio, S.A. Meek, M.J. Abel, L.M. Duffy and G. Meijer, Chem. Phys. Chem. **12**, 1799 (2011).
[8] J.J. Gilijamse, S. Hoekstra, S.A. Meek, M. Metsälä, S.Y.T. van de Meerakker, G. Meijer and G.C. Groenenboom, J. Chem. Phys. **127**, 221102 (2007).
[9] S.A. Meek, G. Santambrogio, B.G. Sartakov, H. Conrad and G. Meijer, Phys. Rev. A **83**, 033413 (2011).
[10] M. Gerhards, Opt. Commun. **241**, 493 (2004).
[11] P.B. Davies and P.A. Martin, Mol. Phys. **70**, 89 (1990).
[12] R. Field, S. Tilford, J. Simmons and R. Howard, J. Mol. Spec. **44**, 347 (1972).
[13] B.G. Wicke, R.W. Field and W. Klemperer, J. Chem. Phys. **56** (12), 5758 (1972).
[14] R.C. Woods and R.J. Saykally, J. Chem. Phys. **89**, 2781 (1988).
[15] J.M. Brown and A. Carrington, *Rotational Spectroscopy of Diatomic Molecules* (Cambridge University Press, Cambridge, 2003).
[16] S.A. Meek, Ph.D. thesis, Freie Universität Berlin, 2010.
[17] R.P. Schwenker, J. Chem. Phys. **42**, 1895 (1965).
[18] M.L. da Silva and M. Dudeck, J. Quant. Spectrosc. Ra. **102**, 348 (2006).